NJC

ROYAL SOCIETY OF CHEMISTRY

PAPER

View Article Online
View Journal | View Issue

Cite this: *New J. Chem.*, 2023, **47**, 5249

The role of carbon dioxide and water in the degradation of zeolite 4A, zeolite 13X and silica gels†

John H. Jacobs, Connor E. Deering, Ruohong Sui, Amelia P. Cann, Kevin L. Lesage and Robert A. Marriott *

Received 6th January 2023,
Accepted 20th February 2023

DOI: 10.1039/d3nj00093a

rsc.li/njc

The degradation of desiccants is important in designing natural gas conditioning processes. Previous studies have focused on the effect of changes in regeneration gas water content, regeneration temperature and number of thermal cycles. However, less is known about how other components impact the lifespan of desiccants over thousands of thermal cycles. Herein we present results on how desiccant degradation is influenced by CO_2 in a process fluid. Increasing the CO_2 concentration resulted in less degradation across unsupported zeolite 4A, zeolite 13X and silica gels. Additionally, higher water concentrations in the regeneration gas resulted in a decrease in the degradation at the same CO_2 concentration. For zeolite 13X, the surface area and pore volumes were larger in the samples subjected to greater CO_2 concentrations. For silica gels, a higher capacity for water adsorption after 5000 thermal swing adsorption cycles was observed in samples with a lower concentration of surface silanol groups.

1. Introduction

Natural gas is an important transitional energy resource. The major components of natural gas from a reservoir are methane (CH_4), hydrogen sulfide (H_2S), carbon dioxide (CO_2) and water (H_2O); additionally, helium (He) and heavier hydrocarbons (such as ethane, C_2H_6, propane, C_3H_8, butane, C_4H_{10}, *etc.*) also can be present in rich natural gas. While the concentrations of natural gas components vary from source to source, the raw natural gas is always saturated with water at the wellhead and after aqueous alkanolamine treatment. This water can lead to pipeline corrosion and possible formation of hydrates during transportation and further processing.[1–5] Therefore, water is removed before transportation in sales gas or before cryogenic liquefaction and can be removed before raw gas gathering lines. Industrially, natural gas is dehydrated through either glycol absorption (at plants and for moderate water dew points) or solid adsorption technology (in the field or within liquid natural gas conditioning), with temperature swing adsorption (TSA) processes being the most common adsorption process.[6–10] In the TSA process, two or three beds are used. Within a three-bed system, one bed dehydrates the raw natural gas stream and a second bed undergoes thermal regeneration to remove the adsorbed water, while a third bed cools, thus allowing for the continuous operation of this system. These adsorption systems are designed for uninterrupted operation over 3-5 years before the desiccants are replaced due to a loss in adsorption capacity.[11–13]

The decrease in adsorption capacity is often attributed to three factors: (I) the collapse of the materials' pores;[14–16] (II) coking of the desiccant materials, thus effectively limiting the adsorption sites of water;[17] and III) the blocking of pores through the condensation of contaminants in the gas stream, such as hydrocarbons.[13] The reaction of aluminum and silica with water is believed to be responsible for changes in the porosity of aluminosilicate zeolites.[18,19] For silica gels, the loss of porosity is attributed to the restructuring of porous silica materials toward non-porous structures in the presence of water and heat, with reported structural changes occurring at temperatures as low as T = 90 °C.[16] Our previous work demonstrated a temperature dependence on the degradation of desiccants, where higher regeneration temperatures result in a greater degree of adsorption capacity loss.[20] Our work also showed that utilizing a wet gas during the thermal regeneration of the desiccants mitigated the degradation of the materials. These results indicate that the major degradation mechanisms are most likely due to (i) mechanical stress from the expansion and contraction of the materials during the heating and cooling steps of the TSA process and (ii) over-stripping the highest energy adsorption sites, thus increasing the rate of crystalline rearrangement.

Department of Chemistry, University of Calgary, 2500 University Drive, N.W., Calgary, AB T2N 1N4, Canada. E-mail: rob.marriott@ucalgary.ca

† Electronic supplementary information (ESI) available: The tabulated data for the capacities of the desiccants over the continuous cycling, and the N_2 physisorption results of the samples. See DOI: https://doi.org/10.1039/d3nj00093a

When comparing the data of our previous experiments, it was observed that experiments where CO_2 was part of the gas mixture, resulted in a lower degree of degradation on zeolite 13X. Thus far, degradation studies on desiccants have been focused on how changes in water concentration and regeneration temperatures impact the degradation of desiccant materials.[18,19] There are no published studies on the role of CO_2 and desiccant material degradation.

In this work, five desiccant materials (zeolite 4A, zeolite 13X, and 2.2 nm, 3.0 nm and 6.0 nm pore size silica gels) were subjected to 5000 TSA cycles at a regeneration temperature of T = 250 °C. Three feed gas phase compositions were investigated for the TSA systems (p_{CO_2} = 3.49 kPa, p_{H_2O} = 2.39 kPa; p_{CO_2} = 3.49 kPa, p_{H_2O} = 2.21 kPa; p_{CO_2} = 34.9 kPa, p_{H_2O} = 2.21 kPa) and the relationship between the wet or dry CO_2 concentrations and amount of degradation was studied.

2. Experimental section

2.1 Materials

The synthesis and characterization of zeolite 4A and 13X materials are reported in our previous publications.[8–10] An in-house EMD Millipore system was used to purify double distilled water to an 18 MΩ cm resistivity. Liquid nitrogen (N_2, 99.998%), helium (He, 99.9990%, Alphagaz 1) and liquid CO_2 (99.8%) were purchased

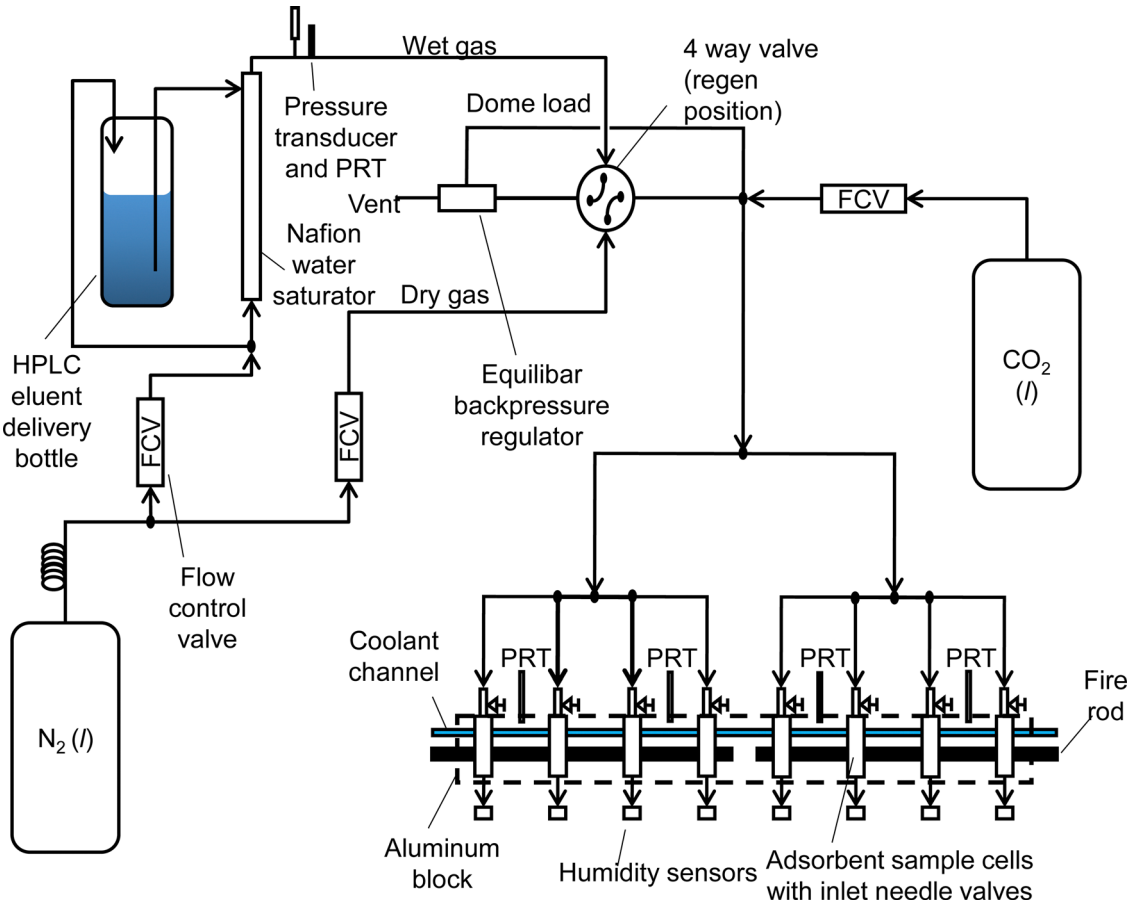

Fig. 1 The schematic of the instrument used during the rapid cycling experiments adapted from the our previous literature.[21]

Table 1 Adsorption and regeneration conditions for the TSA experiments

Experiment	Inlet water content p_{H_2O}/kPa	p_{CO_2}/kPa[b]	p_{total}/kPa[c]	Regeneration feed	Regeneration temperature/°C
I	2.39 ± 0.05	3.49 ± 0.03	349 ± 60	N_2/CO_2	246 ± 9
II	2.39 ± 0.05	3.49 ± 0.03	338 ± 40	$N_2/CO_2/H_2O$[a]	244 ± 8
III	2.21 ± 0.06	34.9 ± 0.3	349 ± 60	N_2/CO_2	246 ± 9
IV	2.21 ± 0.06	34.9 ± 0.3	338 ± 40	$N_2/CO_2/H_2O$[a]	244 ± 8
V	2.21 ± 0.06	3.49 ± 0.03	349 ± 60	N_2/CO_2	246 ± 9
VI	2.21 ± 0.06	3.49 ± 0.03	338 ± 40	$N_2/CO_2/H_2O$[a]	244 ± 8

[a] Regeneration feed and adsorption feed are the same. [b] The CO_2 content was the same for the regeneration feed and adsorption feed. [c] All feeds were balance N_2.

from Air Liquide and used as received. 2.2 nm pore size silica gel (High purity, Davisil Grade 12, 28–200 mesh) and 3.0 nm pore size silica gel (High purity, Davisil Grade 923, 100–200 mesh) were purchased from Sigma Aldrich and used as received. 6.0 nm pore size silica gel (High purity, Davisil Grade 9385, 130–270 mesh) was purchased from Merck and used as received. No binding materials were studied in this work.

2.1.1 Material characterizations. The surface area and pore size distributions of zeolite 13X and the silica gels were characterized by N_2 physisorption using a 3Flex (Micromeritics) instrument. Powder X-ray diffraction (XRD) data were obtained using a Rigaku Multiflex diffractometer with a copper target at a speed of 2° min^{-1} and a step size of 0.02°. The powder XRD patterns were obtained using Jade 7.0 software (International Centre for Diffraction Data, ICDD). Scanning electron microscopy (SEM) and energy dispersive X-ray (EDX) analysis were conducted with an FEI quanta 250 FEG SEM equipped with a GATAN monoCL4 detector. Diffuse reflectance infrared Fourier transform (DRIFT) spectra were obtained by a Varian 7000 FT-IR spectrometer with a diffuse reflectance accessory using Resolutions Pro software. For all DRIFT experiments, samples were placed in a vacuum oven at T = 100 °C for 24 hours and then promptly mixed with potassium bromide (KBr) in a 0.02 : 0.98 sample/KBr mass ratio.

2.2 Water adsorption

Single-point water adsorption measurements were conducted on all materials before and after the TSA cycling experiments using a Thermal Gravimetric Analyser, TGA (TGA 550 Auto apparatus, TA Instruments). The TGA operated by flowing dry He through the balance and the furnace. For the adsorption experiments, the He flowing over the adsorbent was first passed through a water saturator and then diluted by dry He before passing over the adsorbent. The flow rate of He passing through the saturator was controlled using a Brooks SLA5800 mass flow controller. The saturator temperature (T = 15.00 °C) was controlled using a Polyscience chilling circulating bath. During activation, dry He (T = 400 °C, p = 89.05 kPa, at 16 mL min^{-1}) was passed over the adsorbent. The temperature increased at 25 °C min^{-1}, and the sample was held at T = 400 °C for 120 minutes. During the adsorption, 1.4 mole % H_2O in He were held at T = 35 °C, p_{Total} = 89.05 kPa, and 16 mL min^{-1} for 240–360 minutes until a stable mass reading was obtained.

2.3 Rapid thermal swing cycling experiments

To test the materials for their stability in the long-term TSA process, a rapid cycling TSA instrument was used, this instrument was introduced in our previous work[21] (Fig. 1). In each adsorbent

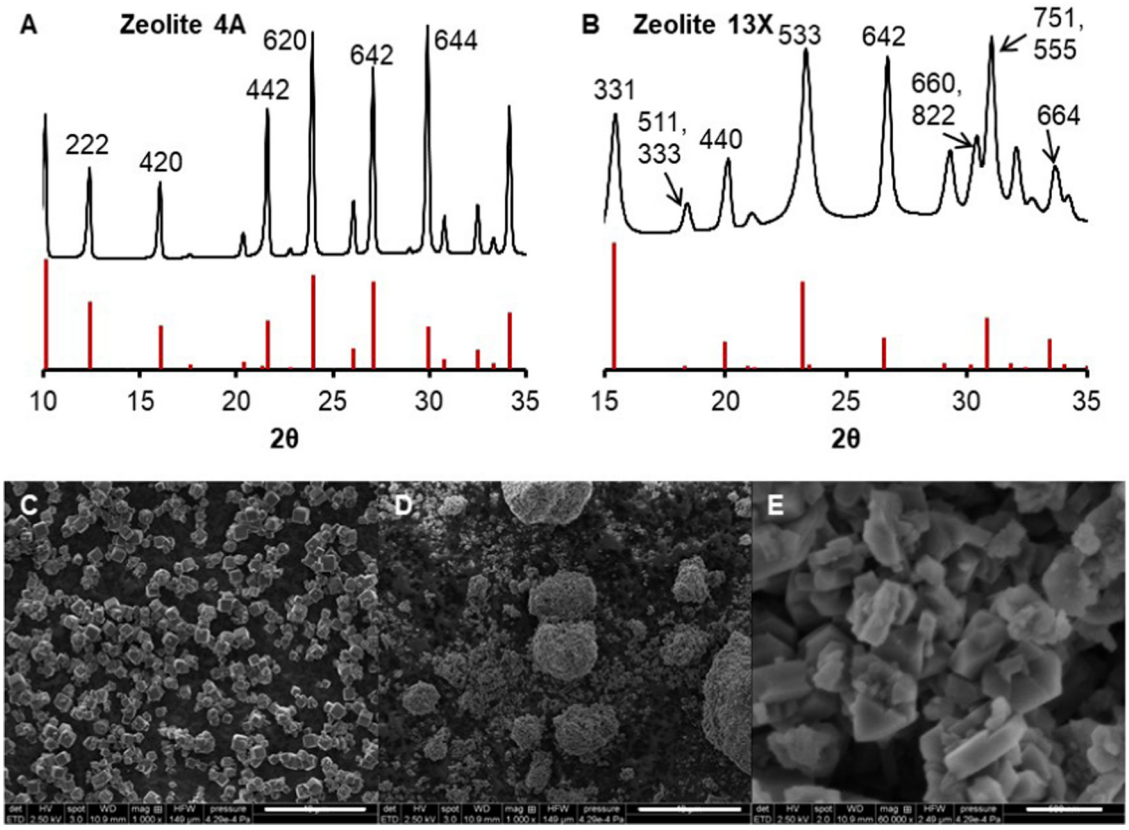

Fig. 2 Powder X-Ray diffraction patterns for zeolite 4A (A) and Zeolite 13X (B). Red lines indicate calculated spectra provided by the International Zeolite Association,[22] and the HKL indices highlighted by the ASTM methods for identifying Linde Type A[23] and Faujasite[24] zeolites are indicated. Scanning electron microscope images of zeolite 4A (C) and zeolite 13X (D and E). The white bars indicate a length of 40 μm (C and D) and the white bar in image E represents a length of 500 nm.

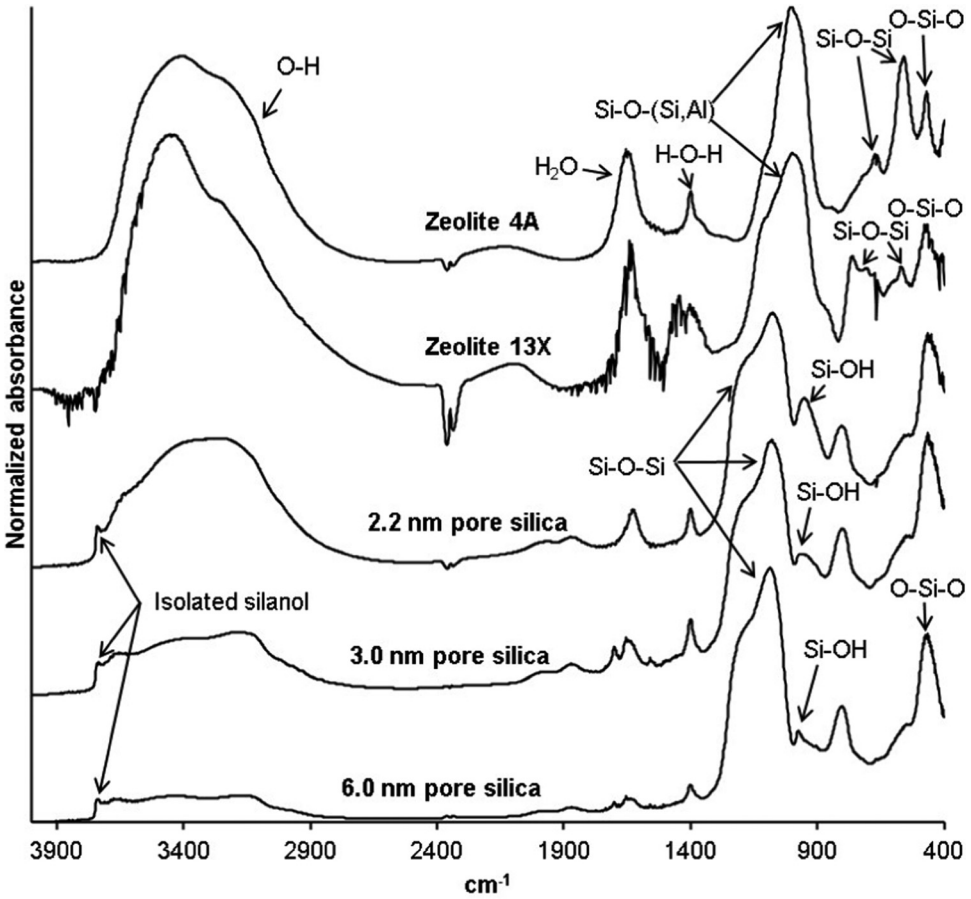

Fig. 3 The DRIFT spectra of the five desiccants.

cell, 25–35 mg of adsorbent material was loaded. For all thermal cycling experiments, the same sequence of events followed:

(a) The adsorbing gas feed flowed through the adsorbent for 330 seconds and was then replaced with the regeneration gas feed.

(b) The block temperature was increased at a rate of 85 °C min^{-1}. Once the desired regeneration temperature was achieved, the block's heating element was cycled on and off to maintain the temperature for 400 seconds.

(c) After the heating time for the adsorbents concluded, the heating elements were switched off, and the water coolant was flowed until the block temperature reached T = 35 °C.

(d) When the block reached a temperature of T = 80 °C, the regeneration feed was replaced with the adsorbing gas feed.

This procedure was repeated until the desired number of cycles was collected. The details of the adsorption and regeneration feed for the experimental conditions can be found in Table 1. The flow rates in each cell were measured using an Agilent Technologies ADM 2000 universal flow meter. As described in our previous work, a Nafion water saturator was used to introduce water into the adsorbing gas feed.[21] The water content of the gas feeds also are present in Table 1.

2.4 Data analysis

2.4.1 Water uptake from breakthrough plot analysis. The detailed methods for the analysis of the rapid cycling data have been presented in our previous work.[21] Two methods were used to track the water uptake for the breakthrough experiments. The first method was to track the change in breakthrough time,

Table 2 Initial water uptake and the specific surface area and pore volumes of the desiccants

	Zeolite 4A	Zeolite 13X	2.2 nm pore silica	3.0 nm pore silica	6.0 nm pore silica
$n^{ads}{}_{H_2O}{}^{a}$/mmol g^{-1}	13.5 ± 0.4	13.5 ± 1.1	6.0 ± 0.7	2.7 ± 0.3	1.80 ± 0.07
$A_{s,BET}$/m^2 g^{-1}	—	589	641	470	453
$V_{pore,total}$/cm^3 g^{-1}	—	0.56	0.45	0.52	1.07
$V_{micropore,t\text{-}plot}$/$cm^3$ g^{-1}	—	0.27	0.10	0	0
$V_{mesopore}$/cm^3 g^{-1}	—	0.02	0.16	0.37	0.57

[a] The amount of water adsorbed at T = 35 °C and p_{H_2O} = 1.25 kPa.

t_b, for each sample as a fraction of the average breakthrough time for the first 30 cycles, $t_b/t_{b,0}$. The breakthrough time could be determined by finding the lowest linearity (R^2) over 25 s. This method of determining the breakthrough time gave a reasonable value for the onset of water content breakthrough and allowed for straightforward automation of the data analysis for large data sets.[21] The second method was to track the change in the integrated area of the regeneration portion of the breakthrough curve, I, as a fraction of the averaged area of the first 30 cycles, I/I_0. The results were then averaged in 50-cycle increments, and the fractions were multiplied by the initial capacity, n_0, obtained from the water adsorption by TGA of the material.

2.4.2 Multiple component regression analysis. A multiple component regression analysis was conducted using the Regression data Analysis tool built into Microsoft Excel was used to test for significance among the different material properties and the adsorption capacities.

$$y = b_0 + \sum_i^N b_i x_i$$

where b_0 is the intercept and b_i is the slope/correlation corresponding to property x_i. A stepwise elimination of the property coefficients was conducted where the coefficient with the lowest magnitude t stat was eliminated until the minimum standard error was achieved. For this analysis, a parameter was only deemed significant if the P-value was below P-value = 0.05.

3. Results and discussion

3.1 Material characterization

The characterization of the zeolite 4A and 13X samples were reported in our other work.[8,9] Using dynamic light scattering, the average particle diameters of zeolites 4A and 13X were determined as 4.45 μm and 21.41 μm, respectively. Through energy dispersive X-Ray analysis, the Si/Al ratios of the zeolites were determined as 1.14–1.15 for zeolite 4A, and 1.8 for zeolite 13X. The scanning electron microscope images (Fig. 2) of the zeolite show that the 4A has large regular crystallites, whereas the 13X are aggregates of smaller crystallites. The powder X-Ray diffraction patterns of the zeolite 4A and 13X materials are shown in Fig. 2, where the experimental peaks are compared to simulated peaks provided by the international zeolite association from the work of Treacy and Higgins.[22] Comparison of the experimental and reference patterns for the two zeolites shows agreement. The diffraction pattern is focused on the range of 10–35 2θ. The significance of this range is it focuses on the HKL peaks used by the ASTM methods to verify the Linde type A,[23] and faujasite diffraction patterns.[24] Both the comparison of the computational patterns and the ASTM methods with the

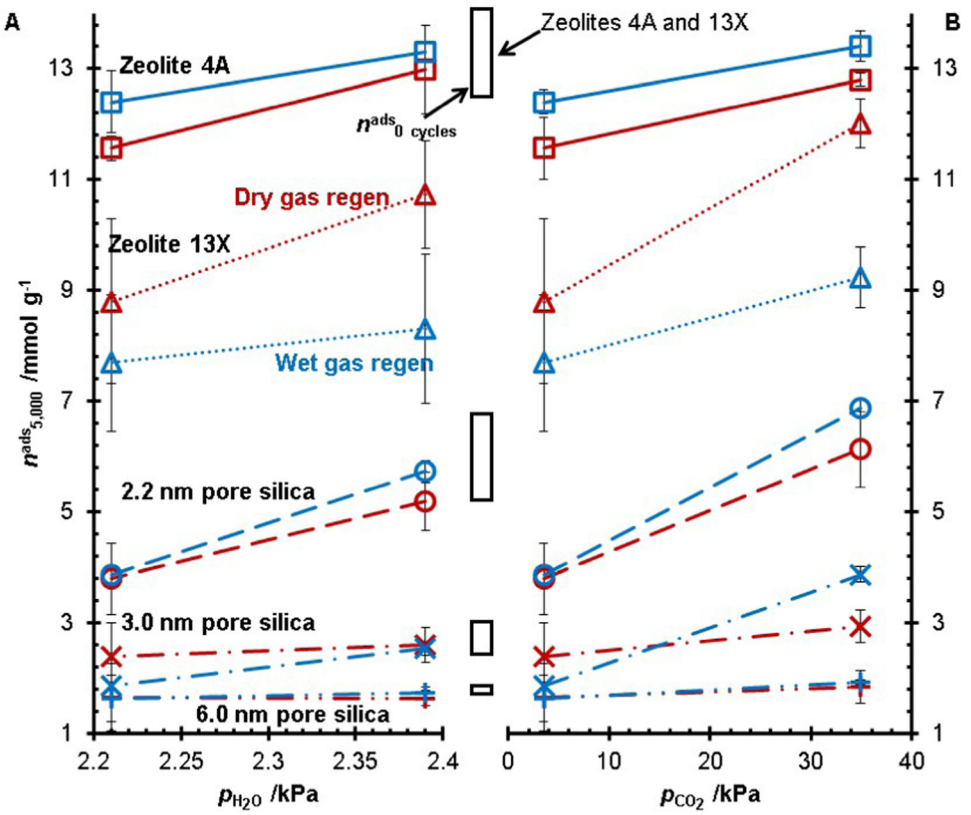

Fig. 4 The capacity after five thousand cycles of zeolite 4A (□, —), zeolite 13X (Δ, • •), 2.2 nm pore size silica (○, — —), 3.0 nm pore size silica (×, — •), and 6.0 nm pore size silica (+, — • •) compared to different water partial pressures at 1% CO_2 (p_{CO_2} = 3.49 kPa) (A) and different CO_2 concentrations at p_{H_2O} = 2.21 kPa. The colours red and blue represent dry gas and wet gas regeneration conditions, respectively, and the black boxes represent the initial uptake of the materials before cycling.

experimental patterns verify the materials to be zeolites 4A and 13X. The silica gels are amorphous materials, thus PXRD was not used to characterize the silicas.

The diffuse reflectance infrared Fourier transform (DRIFT) spectra (Fig. 3) of the zeolites showed a strong OH stretching frequency in the range of 2700–3700 cm^{-1}, likely due to the adsorption of water in the zeolite pores. Peaks at ~1650 cm^{-1} and ~1400 cm^{-1} correspond to water vibration modes.[25] On the zeolite 4A spectra, the peaks at ~983 cm^{-1} (Si–O–Si and Si–O–Al asymmetric stretch), ~670 cm^{-1} (Si–O–Al symmetric stretch), ~550 cm^{-1} (complex vibration band of four member rings), and ~466 cm^{-1} (O–Si–O bending) were observed, all of which are typical of the Linda type A framework.[26] The peaks on zeolite 13X at ~990 cm^{-1} (Si–O–Si and Si–O–Al asymmetric stretch), 760–665 cm^{-1} (complex vibration band of four and six member rings), ~557 and ~500 cm^{-1} (six member ring vibrations), and ~470 cm^{-1} (O–Si–O and O–Al–O bending) also were observed.[26]

Analysis of the DRIFT spectra (Fig. 3) of the silica gels show isolated silanol peaks on all three silica gels at ~3700 cm^{-1}. The silica gels all show similar peaks in the 400–1400 cm^{-1} range with peaks at 1065 cm^{-1} (Si–O–Si stretch), 940 cm^{-1} (Si–OH stretch), 790 cm^{-1} (O–Si–O stretching), 470 cm^{-1} (O–Si–O bending).[27] Comparison of the Si–OH peak at ~940 cm^{-1} between the silica gels shows that the 2.2 nm pore silica had the greatest concentration of silanol groups, while the 6.0 pore size had the least.

The results from TGA analysis of the silica gels showed that the concentration of silanol groups on the 2.2 nm pore size silica gel was 2.5 OH nm^{-2}, the 3.0 nm pore size had 2.3 OH nm^{-2}, and the 6.0 nm pore size had 2.1 OH nm^{-2}. This agrees with the results from the DRIFT spectra. Table 2 shows the results from the single point water adsorption experiments for the five desiccants and the BET specific surface area, total pore volume, *t*-plot micropore volume and mesopore volumes of the three silica gels and zeolite 13X. The Specific surface areas were determined by fitting the BET isotherm equation to the N_2 physisorption isotherm at T = 77 K following the procedure of Brunaur, Emmett, and Teller.[28] The mesopore volumes were determined using the procedure of Barrett *et al.*[29] The micropore volumes were determined using the *t*-plot method.[30]

3.2 Material degradation

The five desiccants studied in this work were subject to 5000 TSA cycles at T_{regen} = 250 °C with the same heating rate across

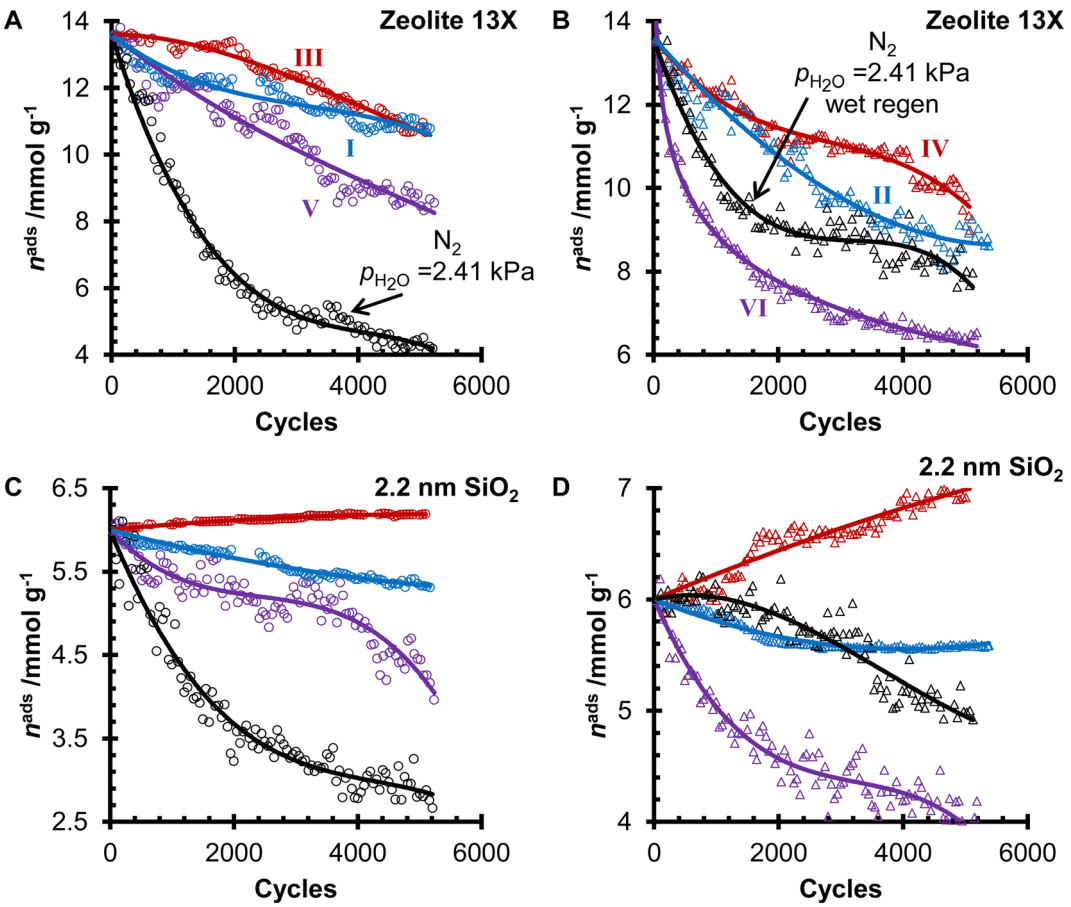

Fig. 5 Capacity changes over 5000 TSA cycles for zeolite 13X (A and B) and the 2.2 nm pore size silica gel (C and D). Results for the dry gas regeneration (A and C) and wet gas regeneration (B and D) experiments are shown. For each material, the results of experiments I (blue, ○), II (blue, Δ), III (red, ○), IV (red, Δ), V (purple, ○), and VI (purple, Δ) were compared to the dry (black, ○) and wet (black, Δ) regeneration conditions of the CO_2 free experiments.[20] For all data sets, solid lines represent empirical polynomial fits to guide the eye.

all experiments. All experiments were run in duplicate for zeolite 4A, zeolite 13X, and the 2.2 nm pore size silica gel. In these experiments, the concentrations of H_2O and CO_2 in the gas feed (adsorption and regeneration) were changed, and the water adsorption capacities after 5000 TSA cycles are shown in Fig. 4. At the same concentration of CO_2, a higher water concentration resulted in a higher water adsorption capacity after 5000 TSA cycles, *i.e.*, less degradation. As well, increasing the CO_2 concentration increased the water capacity of the desiccants after 5000 TSA cycles. Of these two trends, it is noteworthy that the materials subjected to the gas feed with the highest CO_2 concentration had the highest water capacity out of all the experiments. It was observed that for all feed gas streams, zeolite 4A was left with a higher water capacity after 5000 cycles from the wet gas regeneration conditions *versus* the dry gas regeneration conditions. Whereas zeolite 13X consistently had a lower capacity with the wet gas regeneration experiments, the 3.0 nm pore size silica showed inconsistent trends regarding wet gas and dry gas regeneration. For the 2.2 nm and 6.0 nm pore silicas, there was no statistically significant difference between the dry and wet gas regeneration conditions.

To better visualize the changes in the water adsorption capacity during the TSA experiments, the results for zeolite 13X and the 2.2 nm pore size silica gel are shown in Fig. 5. Zeolite 13X and the 2.2 nm pore size silica gel are presented because these are the two materials with the greatest capacity loss from our previous experiments.[20] For the dry gas experiments, the zeolite and the silica gel samples showed greater degradation when no CO_2 was present in the adsorption and regeneration gas feed. For the zeolite 13X, in the wet gas regeneration experiments, the experiment VI condition (p_{CO_2} = 3.49 kPa and p_{H_2O} = 2.21 kPa) showed the greatest capacity loss, followed by the CO_2-free experiment, experiment IV. Finally, experiment II showed the least amount of capacity loss. For the dry regen experiments on the 2.2 nm pore size silica gel, experiments I and V showed similar results during the TSA cycling, but the final measured capacity of the material subjected to experiment V was lower than the results of I. For the dry and wet gas regeneration experiments, capacities during experiments III and IV of the 2.2 nm pore size silica gel increased with the TSA cycling. From this analysis of Fig. 4 and 5, CO_2 changes the desiccant materials' degradation.

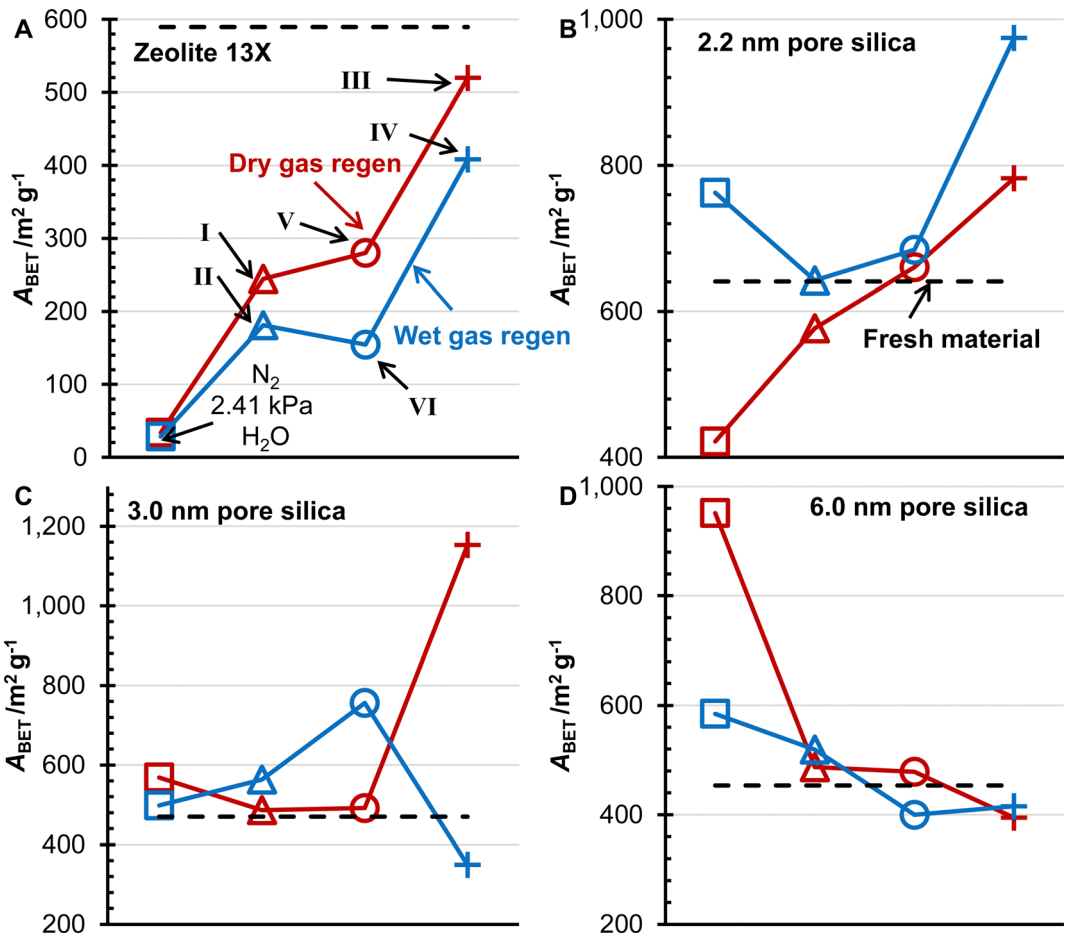

Fig. 6 The BET surface area of zeolite 13X (A), 2.2 nm pore size silica (B), 3.0 nm pore size silica (C), and 6.0 nm pore size silica (D) for the three gas mixtures (p_{CO_2} = 3.49 kPa, p_{H_2O} = 2.39 kPa, Δ; p_{CO_2} = 3.49 kPa, p_{H_2O} = 2.21 kPa, ○; p_{CO_2} = 34.9 kPa, p_{H_2O} = 2.21 kPa, +) and the previously published results (p_{H_2O} = 2.41 kPa, □) without CO_2.[20] Results for dry gas (red) and wet gas (blue) regeneration conditions are reported. The solid black line represents the surface area of the fresh material.

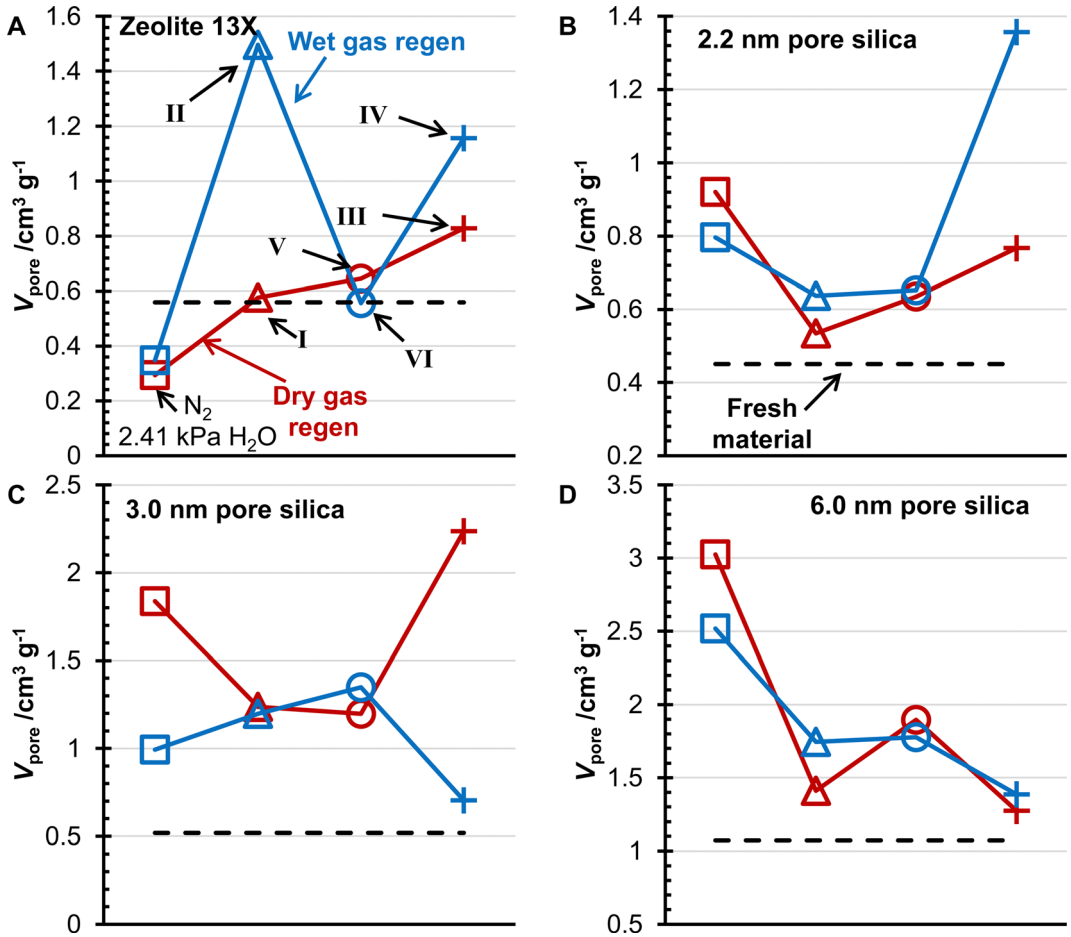

Fig. 7 The pore volumes of zeolite 13X (A), •), 2.2 nm pore size silica (B), 3.0 nm pore size silica (C), and 6.0 nm pore size silica (D) for the three gas mixtures (p_{CO_2} = 3.49 kPa, p_{H_2O} = 2.39 kPa, Δ; p_{CO_2} = 3.49 kPa, p_{H_2O} = 2.21 kPa, ○; p_{CO_2} = 34.9 kPa, p_{H_2O} = 2.21 kPa, +) and the previously published results (p_{H_2O} = 2.41 kPa, □) without CO_2.[20] Results for dry gas (red) and wet gas (blue) regeneration conditions are reported. The solid black line represents the surface area of the fresh material.

Table 3 Specific surface areas and pore volumes of the desiccants after 5000 TSA cycles

Experiment		Zeolite 13X	2.2 nm pore silica	3.0 nm pore silica	6.0 nm pore silica
Fresh sample	$A_{BET}/m^2\ g^{-1}$	589	641	470	951
	$V_{pore}/cm^3\ g^{-1}$	0.56	0.45	0.52	1.07
I	$A_{BET}/m^2\ g^{-1}$	245	577	487	478
	$V_{pore}/cm^3\ g^{-1}$	0.58	0.53	1.24	1.41
II	$A_{BET}/m^2\ g^{-1}$	181	642	563	519
	$V_{pore}/cm^3\ g^{-1}$	1.50	0.64	1.20	1.75
III	$A_{BET}/m^2\ g^{-1}$	520	782	1153	395
	$V_{pore}/cm^3\ g^{-1}$	0.83	0.77	2.24	1.27
IV	$A_{BET}/m^2\ g^{-1}$	408	975	350	415
	$V_{pore}/cm^3\ g^{-1}$	1.16	1.36	0.70	1.39
V	$A_{BET}/m^2\ g^{-1}$	280	660	492	395
	$V_{pore}/cm^3\ g^{-1}$	0.64	0.63	1.20	1.90
VI	$A_{BET}/m^2\ g^{-1}$	155	684	756	400
	$V_{pore}/cm^3\ g^{-1}$	0.56	0.65	1.53	1.78

3.2 Material degradation correlation

The porosity and surface area of the desiccants after 5000 TSA cycles were measured by N_2 physisorption (Fig. 6 and 7). The surface area of zeolite 13X decreased less for the three different gas feeds compared to the N_2/H_2O mixture previously studied.[20] The surface area for the 1% CO_2 (p_{CO_2} = 3.49 kPa) experiments was similar for the two other water contents, while the 10% CO_2 (p_{CO_2} = 3.49 kPa) experiments had the highest surface area for zeolite 13X. This trend was followed for wet and dry gas regeneration conditions, with the wet gas having a lower surface area. The porosity of zeolite 13X showed the same trend as the surface area for the dry gas regeneration conditions. Still, the wet gas conditions showed higher surface areas, and the 1% CO_2 (p_{CO_2} = 3.49 kPa) experiment with a higher water content showed the greatest pore volume. The values of BET specific surface area and pore volumes for the three silica geals and zeolite 13X are presented in Table 3.

Investigating the changes in surface area of the silica gels, the 2.2 nm pore size silica increased in surface area with a decreased water content in the adsorption gas mixture. In contrast, the 10% CO_2 (p_{CO_2} = 34.9 kPa) mixture resulted in the highest surface area of the silica gel. The 3.0 nm pore size silica was observed to have similar surface areas between the N_2/H_2O mixture and the

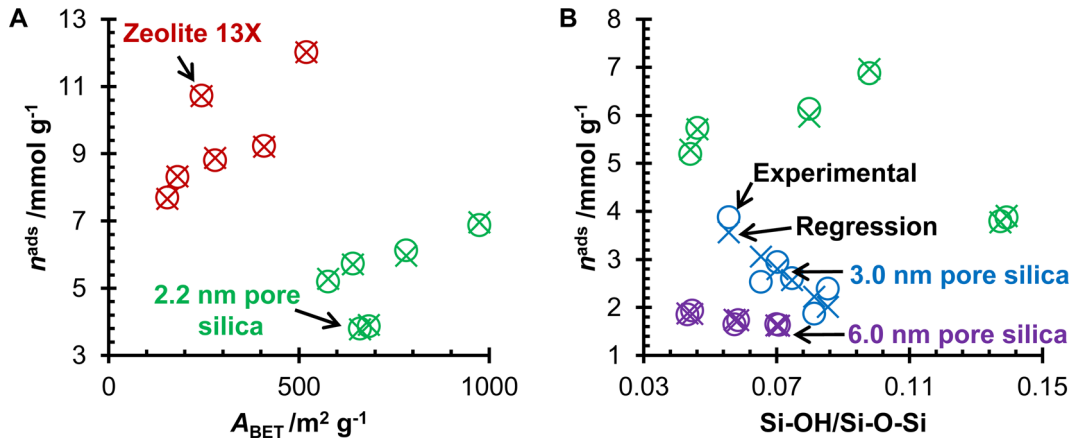

Fig. 8 A comparison of the adsorption capacity of zeolite 13X (red) and 2.2 nm pore size silica (green) against the surface area (A) and the adsorption capacity of the silca gels (2.2 nm pore size, green; 3.0 nm pore size, blue; 6.0 nm pore size, purple) against the ratio of silanol to siloxane groups (B). The experimental capacities (○) and the capacities predicted by the regression analysis (×) are presented for both plots.

1% CO_2 (p_{CO_2} = 3.49 kPa) mixtures for the dry gas regeneration experiments. The surface area increased with decreasing water content for the wet gas regeneration. Interestingly, the surface area for the 10% CO_2 (p_{CO_2} = 34.9 kPa) mixture was the greatest for the dry gas regeneration samples, while the wet gas regeneration showed the lowest surface area. Comparing the N_2/H_2O mixture results for the 6.0 nm pore size silica with the 1% CO_2 (p_{CO_2} = 3.49 kPa) mixtures, it is observed that the surface area decreased with increasing water content for the wet gas regeneration and decreased with increasing CO_2 concentration. The changes in porosity of the 6.0 nm pore size silica followed the same trends as the surface area. For the 6.0 nm pore size, there were no qualitative differences in the surface area and porosity trends between the wet and dry gas regeneration experiments.

The ratio of the silanol groups to the siloxane groups (Si–OH/Si–O–Si) was obtained from DRIFT spectra. The ratio of the silica functional groups was compared to the capacity of the samples after 5000 cycles (Fig. 8B). All three silicas showed a decreased capacity with increasing silanol content. This trend is the opposite expected trend but can be related to the changes in surface area. If the accessible surface area decreases due to the collapse of pores, then even if the silanol groups have been preserved, they will not interact with the water molecules. Additionally, it must be mentioned that there was no evidence in any of the DRFIT spectra to indicate the formation of carboxylate groups on the surface of the desiccants.

A multiple parameter regression analysis was conducted for zeolite 13X and the three silica gel materials to investigate the significance of correlation between the changes in material properties and the changes in adsorption capacities. For zeolite 13X, the BET surface area, pore volume, micropore surface area, and micropore volume all showed significant correlations (P-value < 0.05). Of the tested properties, the correlation to BET surface area showed the largest t-statistic. The plot of capacity against BET surface area is shown in Fig. 8A. For the silica gels, the 2.2 nm pore size silica showed significant correlation between both the BET surface area and the silanol/siloxane ratio (P-value < 0.0005), and both parameters had a similar magnitude t-stat. For the 3.0 and 6.0 nm pore size silicas, only the silanol/siloxane ratio showed a significant correlation (P-value < 0.05).

Interestingly, as the silanol/siloxane ratio increased, the adsorption capacity decreased for all three silica gels. It is already established that the water absorption of silica gels depends on the silanol concentration on the surface of the silica gels, so it stands to reason that increasing the silanol concentration would increase water adsorption. One possible explanation would be that changes in the pore structure reduce the accessibility of water to the silanol groups. It should be noted that the regression fitting of the zeolite 13X properties only had one statistical degree of freedom, while the 2.2 nm pore size silica had three statistical degrees of freedom and the 3.0 and 6.0 nm pore size silicas each had four degrees of freedom.

The crystallinity of the zeolite 4A and zeolite 13X samples was investigated by PXRD (Fig. 9). The dry gas and wet gas regeneration conditions for all three gas mixtures showed little change between the samples. Between the gas mixtures, there was a small amount of peak broadening for the zeolite 4A around 30 2θ. It is difficult to attribute this to changes in the material, as sample preparation can also result in such small changes. We note that peak broadening can be caused by changes in crystallite size and changes in crystallinity. Our previous work showed that zeolite 4A crystals became fractured over time, *versus* loosing crystallinity. The SEM images of the zeolite 4A (Fig. 10) show small particulate around the larger crystallites for all samples, with some of the crystallites showing wear on the surface. However, throughout the imaged samples, there were no indications of fracturing occurring on the crystallites, as was observed in previous experiments without CO_2 in the gas mixture.[20]

The PXRD of zeolite 13X (Fig. 9) showed broadening around the 30 2θ region, but this didn't change between the samples.

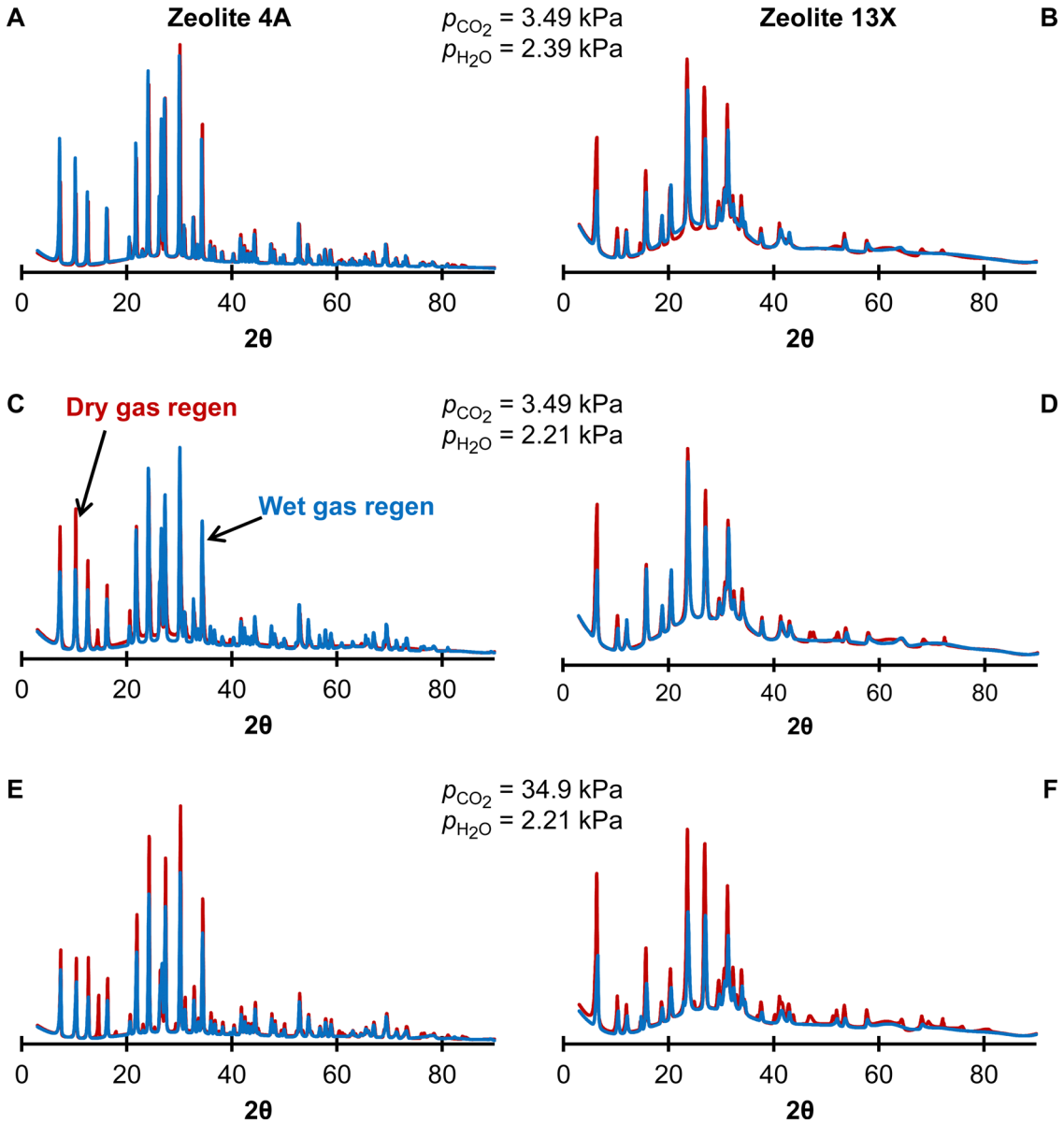

Fig. 9 PXRD spectra for zeolite 4A (Left) and zeolite 13X (Right) for the different gas mixtures (A, B: p_{CO_2} = 3.49 kPa, p_{H_2O} = 2.39 kPa, N_2 balance; C, D: p_{CO_2} = 3.49 kPa, p_{H_2O} = 2.21 kPa, N_2 balance; E, F: p_{CO_2} = 34.9 kPa, p_{H_2O} = 2.21 kPa, N_2 balance). Results for dry gas (red) and wet gas (blue) regeneration conditions are reported.

Unlike the experiments without CO_2 in the gas mixture,[20] the zeolite generally retained crystallinity without much difference between the dry and wet gas regeneration conditions. The SEM images (Fig. 11) of the zeolite 13X samples after 5000 TSA cycles showed that all six samples retained sharp edges of the crystallites, whereas the images from the experiments without CO_2 in the gas mixture[20] showed rounding of the crystallite edges.

The adsorption mechanism of CO_2 on both zeolite and silica surfaces is believed to be primarily physisorption, with some studies indicating a minor amount of chemisorption occurring on these materials.[31,32] The presence of the chemisorbed CO_2 could inhibit the degradation of the desiccants during the TSA cycling. For the silica gel materials, the CO_2 may interfere with the dehydroxylation/rehydroxylation process during thermal treatment. It is known that silanols on silica surfaces are lost during thermal treatment, and that when water is present, the silanols can be regenerated on the silica surface.[33] To better understand the role of CO_2 on the surface silanol chemistry, further experiments will need to be conducted.

4. Conclusion

The previous literature[18,19] into what factors influence the degradation of desiccants have always focused on changes in

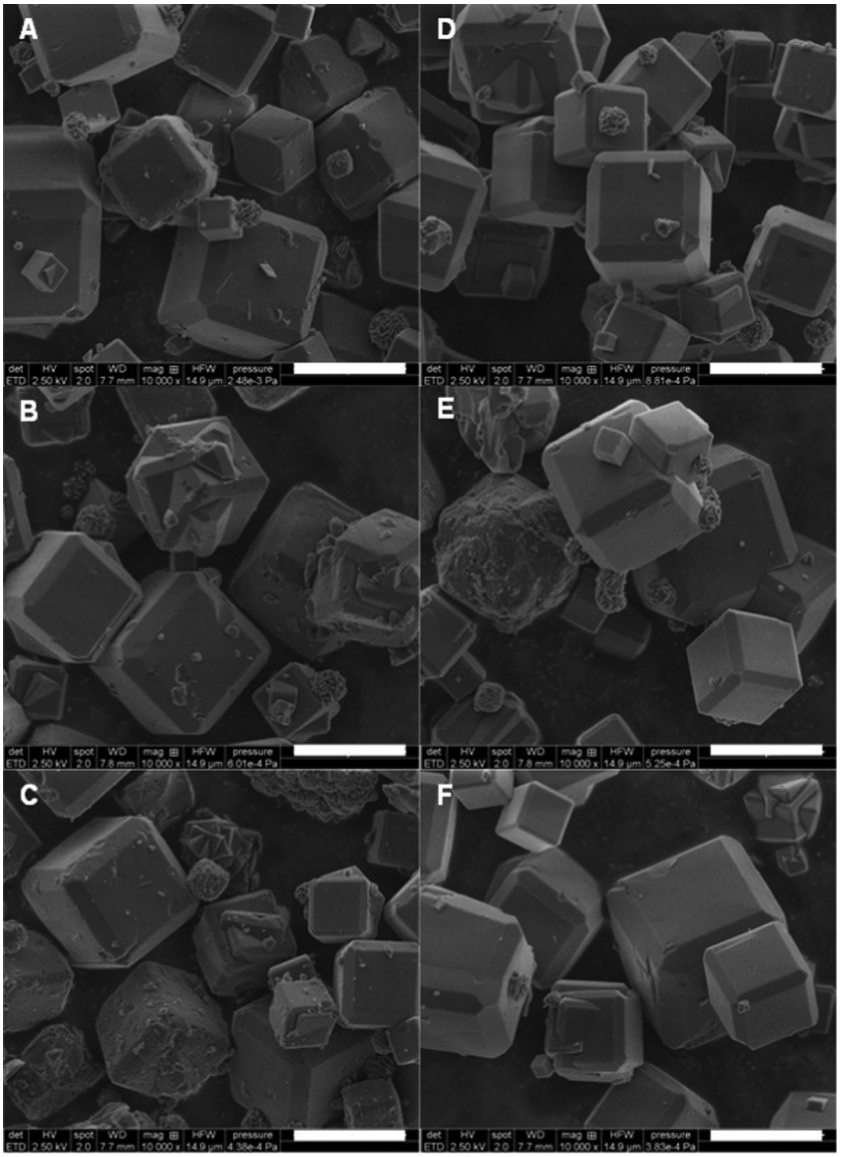

Fig. 10 SEM images of zeolite 4A after 5000 TSA cycles. Images for (A, D: p_{CO_2} = 3.49 kPa, p_{H_2O} = 2.39 kPa, N_2 balance; B, E: p_{CO_2} = 3.49 kPa, p_{H_2O} = 2.21 kPa, N_2 balance; C, F: p_{CO_2} = 34.9 kPa, p_{H_2O} = 2.21 kPa, N_2 balance). Images of the material after dry gas (A–C) and wet gas (D–F) regeneration conditions are presented. The white bars represent a length of four μm.

water content or regeneration temperature. We present results on how the degradation of desiccants is influenced by the concentration of CO_2 in the process fluid. It was observed that increasing the CO_2 concentration (in the regeneration gas) resulted in less degradation across all desiccants tested. Additionally, higher water concentrations in the regeneration gas resulted in a decrease in the desiccant degradation at the same CO_2 concentration. For zeolite 13X, the surface area and pore volumes were greater in the samples subjected to a 10% CO_2 (p_{CO_2} = 34.9 kPa) gas mixture during the TSA process than in the 1% CO_2 (p_{CO_2} = 3.49 kPa) mixtures. In the silica gel samples, a higher capacity for water adsorption after 5000 TSA cycles was observed in materials with a lower concentration of surface silanol groups, *i.e.*, silica gel became a better adsorbent upon exposure to hot wet CO_2. As expected, higher surface areas were associated with higher adsorption capacities.

In terms of looking at the degradation of commercial desiccants, these results are important for materials applications in different process scenarios. For example, dehydration for the purposes of cryogenic liquefaction of natural gas would not benefit from CO_2, but could benefit from wet gas regeneration. Alternatively, raw gas conditioning at the wellhead would benefit from the presence of CO_2, H_2O in the regeneration gas and a lower regeneration temperature (lower dew-point requirements). Future work should consider the effect of binders, which will be challenging for 5000 cycles. Here the rapid cycling is possible due to the small beds explored, whereas larger tests require both

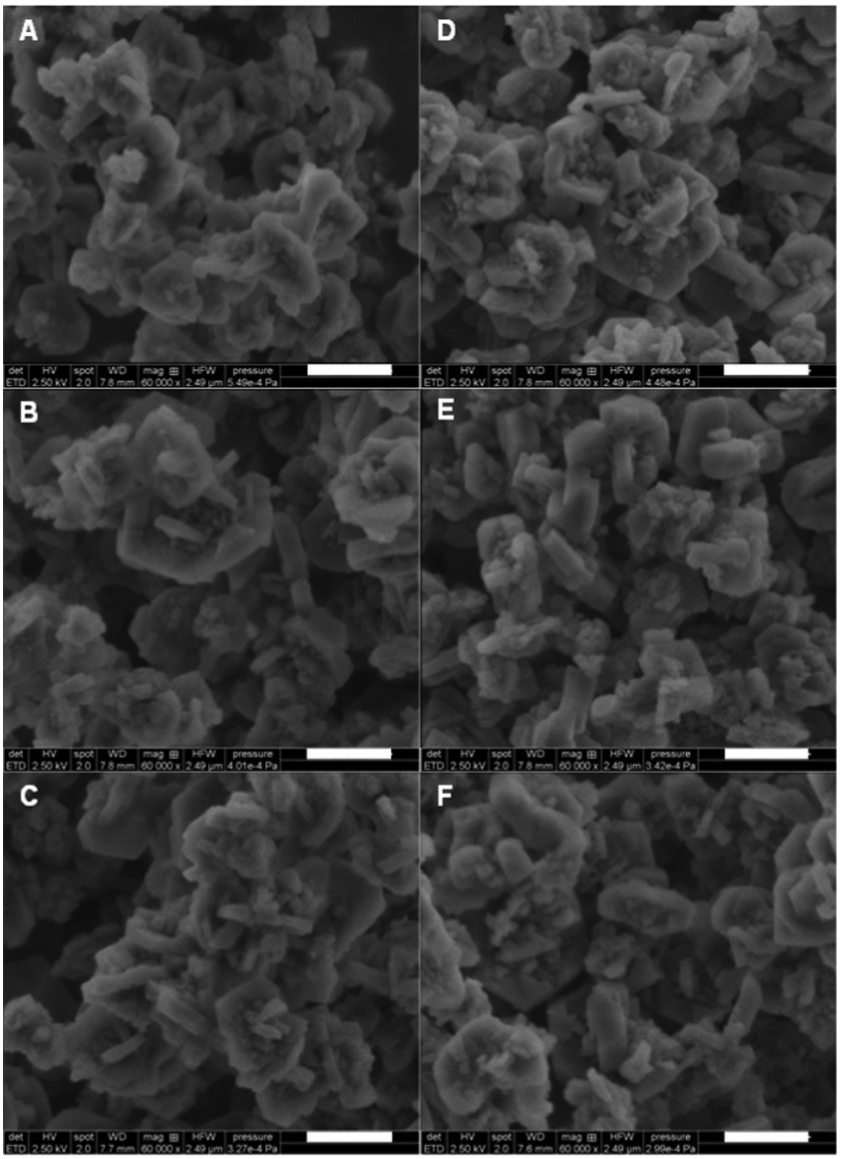

Fig. 11 SEM images of zeolite 13X after 5000 TSA cycles. Images for (A and D: p_{CO_2} = 3.49 kPa, p_{H_2O} = 2.39 kPa, N_2 balance; B and E: p_{CO_2} = 3.49 kPa, p_{H_2O} = 2.21 kPa, N_2 balance; C and F: p_{CO_2} = 34.9 kPa, p_{H_2O} = 2.21 kPa, N_2 balance). Images of the material after dry gas (A–C) and wet gas (D–F) regeneration conditions are presented. The white bars represent a length of 500 nm.

large laboratory gas flow and longer experimental time (years *versus* months).

Conflicts of interest

The authors declare no competing financial interest.

Acknowledgements

The funding for this research was provided through the Natural Science and Engineering Research Council of Canada (NSERC) and Alberta Sulphur Research Ltd. (ASRL) Industrial Research Chair in Applied Sulfur Chemistry. In addition to NSERC, the authors are grateful to the feedback from the member companies of ASRL.

References

1 A. L. Kohl and R. Nielsen, *Gas purification*, Gulf Pub, Houston, Tex, 5th edn, 1997.
2 Z. T. Ward, R. A. Marriott, A. K. Sum, E. D. Sloan and C. A. Koh, Equilibrium Data of Gas Hydrates containing Methane, Propane, and Hydrogen Sulfide, *J. Chem. Eng. Data*, 2015, **60**, 424–428.
3 S. Zarinabad and A. Samimi, Problems of Hydrate Formation in Oil and Gas Pipes Deals, *J. Am. Sci.*, 2012, **8**, 1007–1010.

4 P. Gandhidasan, A. A. Al-Farayedhi and A. A. Al-Mubarak, Dehydration of natural gas using solid desiccants, *Energy*, 2001, **26**, 855–868.
5 L. Popoola, A. Grema, G. Latinwo, B. Gutti and A. Balogun, Corrosion problems during oil and gas production and its mitigation, *Int. J. Ind. Chem.*, 2013, **4**, 35.
6 R. W. Baker and K. Lokhandwala, Natural Gas Processing with Membranes: An Overview, *Ind. Eng. Chem. Res.*, 2008, **47**, 2109–2121.
7 J. M. Campbell and R. N. Maddox, *Gas conditioning and Processing: Gas Treating and Sulfur Recovery*, Campbell Petroleum Series, Norman, Okla, 4th edn, 1998.
8 K. G. Wynnyk, B. Hojjati, P. Pirzadeh and R. A. Marriott, High-pressure sour gas adsorption on zeolite 4A, *Adsorption*, 2017, **23**, 149–162.
9 K. G. Wynnyk, B. Hojjati and R. A. Marriott, High-Pressure Sour Gas and Water Adsorption on Zeolite 13X, *Ind. Eng. Chem. Res.*, 2018, **57**, 15357–15365.
10 K. G. Wynnyk, B. Hojjati and R. A. Marriott, Sour Gas and Water Adsorption on Common High-Pressure Desiccant Materials: Zeolite 3A, Zeolite 4A, and Silica Gel, *J. Chem. Eng. Data*, 2019, **64**, 3156–3163.
11 Gas Processors Supplier's Assoc. (GPSA), *Engineering Data Book*, Tulsa, OK, 1987.
12 R. H. Herold and S. Mokhatab, Optimal design and operation of molecular sieves for gas dehydration-Part 1, *Gas Process.*, 2017, **96**, 25–30.
13 R. H. Herold and S. Mokhatab, Optimal design and operation of molecular sieves for gas dehydration-part 2, *Gas Process.*, 2017, **96**, 33–36.
14 D. M. Ruthven, *Principles of adsorption and adsorption processes*, Wiley, New York, 1984.
15 C. Li, W. Jia and X. Wu, Experimental Failure-Mechanism Analysis of 4A Zeolites Used for Natural-Gas Drying, *Chem. Technol. Fuels Oils*, 2015, **51**, 245–251.
16 W. Lutz, M. Weber, R. Bertram, R. Kurzhals and G. Kryukova, The Ageing of Silica Gels Affected by Hydrothermal Treatment, *Z. Anorg. Allg. Chem.*, 2011, **637**, 421–425.
17 R. Gomes Santiago, B. Ferreira dos Santos, I. Gomes Lima, K. Oliveira Moura, D. Carrijo Melo, W. Mantovani Grava, M. Bastos-Neto, S. M. Pereira de Lucena and D. Cristina Silva de Azevedo, Invstigation of premature aging of zeolites used in the drying of gas streams, *Chem. Eng. Commun.*, 2019, **206**, 1367–1374.
18 M. Suckow, W. Lutz, J. Kornatowski, M. Rozwadowski and M. Wark, Calculation of the hydrothermal long-term stability of zeolites in gas-desulphurization and gas-drying processes, *Gas Sep. Purif.*, 1992, **6**, 101–108.
19 C. J. Heard, L. Grajciar, F. Uhlík, M. Shamzhy, M. Opanasenko, J. Čejka and P. Nachtigall, Zeolite (In)Stability under Aqueous or Steaming Conditions, *Adv. Mater.*, 2020, **32**, 2003264.
20 J. H. Jacobs, C. E. Deering, R. Sui, K. L. Lesage and R. A. Marriott, Degradation of desiccants in temperature swing adsorption processes: The temperature dependent degradation of zeolites 4A, 13X and silica gels, *Chem. Eng. J.*, 2023, **451**, 139049.
21 J. H. Jacobs, C. E. Deering, K. L. Lesage, M. J. Stashick and R. A. Marriott, Rapid Cycling Thermal Swing Adsorption Apparatus: Commissioning and Data Analyses for Water Adsorption of Zeolites 4A and 13X Over 2000 Cycles, *Ind. Eng. Chem. Res.*, 2021, **60**, 7487–7494.
22 M. M. J. Treacy and J. B. Higgins, *Collection of simulated XRD powder patterns for zeolites*, Elsevier, Amsterdam, Boston, 5th rev. edn, 2007.
23 D32 Committee, *Test Method for Determination of Relative Crystallinity of Zeolite Sodium A by X-ray Diffraction*, ASTM International.
24 D32 Committee, *Test Method for Determination of Relative X-ray Diffraction Intensities of Faujasite-Type Zeolite-Containing Materials*, ASTM International.
25 T. Seki, K.-Y. Chiang, C.-C. Yu, X. Yu, M. Okuno, J. Hunger, Y. Nagata and M. Bonn, The Bending Mode of Water: A Powerful Probe for Hydrogen Bond Structure of Aqueous Systems, *J. Phys. Chem. Lett.*, 2020, **11**, 8459–8469.
26 W. Mozgawa, M. Król and B. Katarzyna, *Chemik*, 2011, **65**, 667–674FT-IR studies of zeolites from different structural groups.
27 L. B. Cappeletti, E. Moncada, J. Poisson, I. S. Butler and J. H. Z. D. Santos, Determination of the Network Structure of Sensor Materials Prepared by Three Different Sol-Gel Routes Using Fourier Transform Infrared Spectroscopy (FT-IR), *Appl. Spectrosc.*, 2013, **67**, 441–447.
28 S. Brunauer, P. H. Emmett and E. Teller, Adsorption of Gases in Multimolecular Layers, *J. Am. Chem. Soc.*, 1938, **60**, 309–319.
29 E. P. Barrett, L. G. Joyner and P. P. Halenda, The Determination of Pore Volume and Area Distributions in Porous Substances. I. Computations from Nitrogen Isotherms, *J. Am. Chem. Soc.*, 1951, **73**, 373–380.
30 B. Lippens, Studies on pore systems in catalysts V. The t method, *J. Catal.*, 1965, **4**, 319–323.
31 P. Rzepka, Z. Bacsik, A. J. Pell, N. Hedin and A. Jaworski, Nature of Chemisorbed CO_2 in Zeolite A, *J. Phys. Chem. C*, 2019, **123**, 21497–21503.
32 R. Roque-Malherbe, R. Polanco-Estrella and F. Marquez-Linares, Study of the Interaction between Silica Surfaces and the Carbon Dioxide Molecule, *J. Phys. Chem. C*, 2010, **114**, 17773–17787.
33 L. T. Zhuravlev, The surface chemistry of amorphous silica. Zhuravlev model, *Colloids Surf., A*, 2000, **173**, 1–38.